J. Fluid Mech. (2007), *vol.* 577, *pp.* 495–505.
doi:10.1017/S0022112007005174 Printed in the United Kingdom

The effect of confining boundaries on viscous gravity currents

DAISUKE TAKAGI AND HERBERT E. HUPPERT

Institute of Theoretical Geophysics, Department of Applied Mathematics and Theoretical Physics, University of Cambridge, Centre for Mathematical Sciences, Wilberforce Road, Cambridge CB3 0WA, UK

(Received 29 November 2006 and in revised form 19 January 2007)

Newtonian viscous gravity currents propagating along horizontal and inclined channels with semicircular and V-shaped boundaries are examined. Similarity solutions are obtained from the governing mathematical equations and compared with closely matching data from laboratory experiments in which the propagation of glycerine along different channels was recorded. Geological applications of the results are discussed briefly.

1. Introduction

Gravity currents are flows driven by gravity due to horizontal differences in density between two fluids. Examples include oil spreading over water, honey spreading over toast and sea breezes spreading over land. Seafloor turbidity currents, lahars, and lava flows are further examples, all of geological relevance (Simpson 1997; Huppert 2006).

Here, we consider the propagation and evolution of low-Reynolds-number flows. In previous publications, two-dimensional viscous gravity currents flowing axisymmetrically above a horizontal surface (Huppert 1982*a*), down a slope (Huppert 1982*b*) and over a deep porous medium (Acton, Huppert & Worster 2001) have been studied analytically and the results tested experimentally. Numerous variations exist on this general theme. For example, Mei & Yuhi (2001) studied numerically the flow of a Bingham fluid in a sloping confined channel, while Lister (1992) determined the flow of a Newtonian fluid on an inclined plane from a point or line source. In this paper, we consider viscous flows along confined channels of different cross-sectional shapes to investigate the influence of bottom boundaries on the flow features. The main motivations of our study are to develop and understand the underlying structure of solutions, test them experimentally, and apply them to problems including lava flows propagating down confined channels. Of particular interest is the extent to which boundary shapes affect the flow rate and velocity profile of the propagating viscous fluid. Our aim is to explore how different confining boundaries give rise to different propagation rates and forms of gravity currents.

We consider the flow along smooth channels with uniform cross-section, neglecting surface tension effects (large Bond number). Two cross-sectional shapes are considered: semicircular and V-shaped boundaries. In the next section we set up a theoretical framework and derive mathematical solutions. Similarity solutions for the propagating distance as functions of time are obtained for the two boundary shapes. With an instantaneous release of a fixed volume of fluid into a semicircular cross-section, the propagating distance scales as $t^{1/4}$ for non-inclined and $t^{3/7}$ for

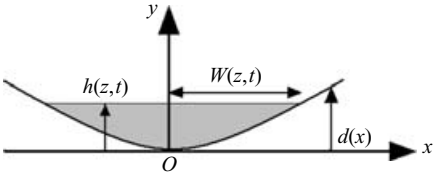

FIGURE 1. Sketch of a cross-section of an arbitrary channel.

inclined channels, regardless of the angle of inclination. For V-shaped boundaries, the distance scales as $t^{2/7}$ for non-inclined and $t^{1/2}$ for inclined channels, again independent of the angle of inclination. These scalings hold independently of the angle at the vertex. We note that the results significantly differ from two-dimensional and axisymmetric geometries in the horizontal, where propagation distance scales like $t^{1/5}$ and $t^{1/8}$ respectively (Huppert 1982*a*). Two-dimensional flows down a slope propagate like $t^{1/3}$ (Huppert 1982*b*). All these results are summarized in table 1 in § 2. In § 3, the theoretical results are found to be in close agreement with data from laboratory experiments. We conclude by discussing implications of our results for geological applications.

2. Theory

2.1. *Geometrical set-up*

Consider a low-Reynolds-number flow of a viscous, incompressible, Newtonian fluid of kinematic viscosity ν and uniform density ρ initially at rest at one closed end of an arbitrary channel of cross-section $y = d(x)$, with respect to mutually perpendicular Cartesian axes, with x across the channel, y normal to the slope and z along the channel. The channel makes an angle β with the horizontal and the fluid is released at time $t = 0$. A short time after the release, a thin layer of viscous fluid propagates slowly along the channel. We treat the width of the fluid at the top $2W(z, t)$ and the fluid height $h(z, t)$ as slowly varying functions of z only. The length scale in the x-direction is very small compared to that in the z-direction once the fluid has propagated sufficiently to occupy the width of the channel, so h is independent of x as shown in the sketch of a typical cross-section in figure 1.

We begin by computing the hydrostatic pressure p in the current as

$$p = p_0 + \rho g(h - y)\cos\beta, \tag{2.1}$$

where $p = p_0$ is the constant atmosperic pressure on the free surface $y = h$. The fluid has non-zero velocity component only in the z-direction, denoted by u.

We proceed by substituting (2.1) into the Stokes equation (Batchelor 1967)

$$0 = -\nabla p + \boldsymbol{F} + \mu\nabla^2\boldsymbol{u}, \tag{2.2}$$

where μ is the dynamic viscosity, and $\boldsymbol{F}$ the body force per unit volume, to obtain the governing differential equation for u

$$\frac{\partial^2 u}{\partial x^2} + \frac{\partial^2 u}{\partial y^2} = -M, \tag{2.3}$$

where M, which is dependent on the inclination angle β, is given by

$$M = -\frac{g}{\nu}\frac{\partial h}{\partial z} \quad (\beta = 0),\ M = \frac{g}{\nu}\sin\beta \quad (\beta \neq 0). \tag{2.4a,b}$$

The apparent discontinuity at $\beta = 0$ is due to (2.4*b*) only being valid if the angle of the incline is not too small, so that the current is driven by the component of gravity down the slope, rather than by the slope of the free surface. The formal condition for that is $|\partial h/\partial z| \ll \tan\beta$.

There are two boundary conditions. First, the fluid does not slip on the rigid surface $y = d$. Secondly, the tangential stress vanishes on the free surface $y = h$. Mathematically, these become

$$u = 0 \quad (y = d), \; \partial u/\partial y = 0 \quad (y = h). \tag{2.5a,b}$$

When the length scale of fluid height h is much smaller than that of width W, the first term in (2.3) can be neglected and it suffices to deal with the modified equation $\partial^2 u/\partial y^2 = -M$, which with the boundary conditions (2.5*a*, *b*) admits the unique solution

$$u = \tfrac{1}{2}M(2h - d - y)(y - d). \tag{2.6}$$

This neglect of the x-derivative is valid when the bottom boundary is semicircular, but not when it is V-shaped. We consider the two problems separately, with a semicircular cross-section in § 2.2 and a V-shaped boundary in § 2.3.

Once the velocity profile is determined, we derive a partial differential equation from the local continuity equation (Acheson 1990)

$$\frac{\partial A}{\partial t} + \frac{\partial Q}{\partial z} = 0, \tag{2.7}$$

where the cross-sectional area occupied by the flow if $d(x)$ is an even function of x is

$$A(z, t) = 2\int_0^{W(z,t)} [h(z, t) - d(x)]\,\mathrm{d}x \tag{2.8}$$

and the downstream volume flux is

$$Q(z, t) = 2\int_0^{W(z,t)} \mathrm{d}x \int_{d(x)}^{h(z,t)} u(x, y, z, t)\,\mathrm{d}y. \tag{2.9}$$

Differentiating the definition of A with respect to t, we can rewrite (2.7) as

$$2W\frac{\partial h}{\partial t} + \frac{\partial Q}{\partial z} = 0. \tag{2.10}$$

An additional boundary condition is the global continuity equation

$$\int_0^{z_N(t)} A\,\mathrm{d}z = V, \tag{2.11}$$

where $z_N(t)$ is the length of the current at time t and V is the released volume of fluid. In the horizontal case, we also impose the condition $h\big[z_N(t), t\big] = 0$, that the height of the current vanishes at the front $z = z_N$ (Huppert 1982*a*). In the inclined situation, the order of the governing differential equation is lower and no boundary condition is specified at the front of the current whose position is determined by (2.11) (Huppert 1982*b*).

An immediate question is whether there is a similarity solution to (2.3)–(2.11). The argument against the existence of a similarity solution is that, in contrast to the previous flows studied (Huppert 1982*a*, *b*, 2006), there is the added length scale of the channel. The argument in favour is that the depth of the current $h - d$ is generally very much smaller than W and so the additional length scale introduced should be irrelevant. The second argument is correct.

2.2. *Semicircular cross-section*

For semicircular cross-section with radius of curvature a, we have $d = a-(a^2-x^2)^{1/2}$. The length scale x is much smaller than a so $d \simeq x^2/2a$, and the velocity profile from (2.6) is

$$u = \frac{M}{2}\left(2h - \frac{x^2}{2a} - y\right)\left(y - \frac{x^2}{2a}\right). \tag{2.12}$$

A simple check reassures us that the condition of the second term dominating the first in (2.3) is equivalent to $-3x^2/a^2 + 2h/a \ll 1$ which is consistent with $|x|, h \ll a$ in thin layer flows.

The volume flux Q over the cross-sectional area $A = \frac{4}{3}(2ah^3)^{1/2}$ is obtained as

$$Q = \int_A u \,\mathrm{d}x\,\mathrm{d}y = \frac{32\sqrt{2}}{105} M a^{1/2} h^{7/2}. \tag{2.13}$$

Expressions for Q and A are substituted into the local continuity equation (2.7) to obtain

$$h^{1/2}\frac{\partial h}{\partial t} + \frac{16}{105}\frac{\partial}{\partial z}\left(Mh^{7/2}\right) = 0. \tag{2.14}$$

In the non-inclined case $\beta = 0$, we choose a similarity variable

$$\eta = \left(\frac{70\nu a}{3gV^2}\right)^{1/4} z t^{-1/4} \tag{2.15}$$

and seek a similarity solution $h(z, t)$ of the form

$$h = \eta_N^{2/3}\left(\frac{945\nu V^2}{512gat}\right)^{1/6}\phi(w), \tag{2.16}$$

where $w = \eta/\eta_N$, η_N being a dimensionless constant corresponding to the value of η at the end point of the current, and the various numerical prefactors in (2.15) and (2.16) have been chosen to simplify the resulting differential equations and subsidiary conditions. It is immediately seen from (2.15) that z_N increases like $t^{1/4}$.

To evaluate η_N explicitly, and the corresponding structure of the flow, we substitute (2.15) and (2.16) into (2.14) and (2.11) to obtain

$$\left(\phi'\phi^{7/2}\right)' + \tfrac{1}{2}\phi^{1/2}\left(\tfrac{1}{3}\phi + \tfrac{1}{2}w\phi'\right) = 0 \tag{2.17}$$

and

$$\eta_N = \left(\int_0^1 \phi^{3/2}(w)\,\mathrm{d}w\right)^{-1/2}, \tag{2.18}$$

alongside the boundary condition $\phi(1) = 0$. The solutions are found by direct integration to be $\phi(w) = [\frac{1}{4}(1 - w^2)]^{1/3}$ and $\eta_N = 2\sqrt{2/\pi}$. Hence, the fluid height is given by

$$h = \frac{1}{4}\left[105\nu\left(z_N^2 - z^2\right)/g\right]^{1/3} t^{-1/3} \quad \text{where} \quad z_N = 2\left(\frac{6gV^2}{35\pi^2\nu a}\right)^{1/4} t^{1/4}. \tag{2.19a,b}$$

In the inclined case, the governing differential equation becomes

$$\frac{\partial h}{\partial t} + \frac{8g\sin\beta}{15\nu} h^2 \frac{\partial h}{\partial z} = 0. \tag{2.20}$$

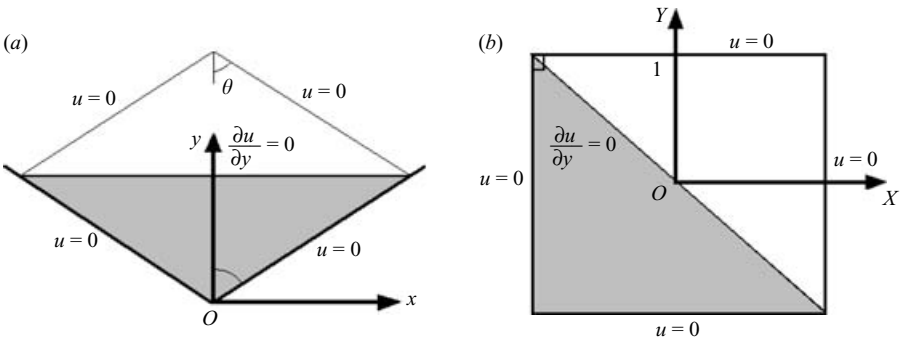

FIGURE 2. The geometry and boundary conditions in the (*a*) (*x*,*y*)- and (*b*) (*X*,*Y*)-planes.

From the results for the flow down a two-dimensional slope (Huppert 1982*b*), it follows immediately that the solution for $h(z, t)$ is

$$h = \left(\frac{15\nu}{8g\sin\beta}\right)^{1/2} z^{1/2} t^{-1/2} \qquad (0 < z < z_N) \tag{2.21}$$

with z_N evaluated from the constraint (2.11) given by

$$z_N = \frac{1}{2}\left(\frac{3(7V)^4 g^3 \sin^3\beta}{(5\nu)^3(2a)^2}\right)^{1/7} t^{3/7}. \tag{2.22}$$

We deduce that along an inclined channel, z_N scales like $t^{3/7}$, and the dependence on the inclination angle β only appears in the pre-multiplicative factor. It is interesting that the form of the free surface height (2.21) is independent of the scale of the constraining boundary, a, and of V, both of which only enter the rate of propagation of the current as represented by (2.22).

2.3. *V-shaped boundary*

Consider now a V-shaped boundary with sidewalls meeting at an angle 2θ at the vertex, so that the bottom boundary is given by $d = |x|/\tan\theta$. Neglecting one of the left-hand-side terms in the differential equation (2.3) is only suitable for special cases, namely for θ close to 0 or $\pi/2$, so a different method is needed for general θ. With reference to figure 2(*a*), we satisfy the boundary condition of zero vertical gradient at the free surface $y = h$ by determining the symmetric solution of the governing equation in the diamond geometry shown after imposing $u = 0$ on the whole boundary. The differential equation is then more easily solved in terms of new coordinates (sketched in figure 2*b*)

$$X = \frac{1}{h}\left(y + \frac{x}{m}\right) - 1, \quad Y = \frac{1}{h}\left(y - \frac{x}{m}\right) - 1, \tag{2.23a,b}$$

where $m = \tan\theta$. The differential equation (2.3) becomes

$$(m^2+1)\left(\frac{\partial^2 u}{\partial X^2} + \frac{\partial^2 u}{\partial Y^2}\right) + 2(m^2-1)\frac{\partial^2 u}{\partial X \partial Y} = -Mm^2h^2. \tag{2.24}$$

We posit a solution in the form

$$u = \sum_{i=0}^{\infty}\sum_{j=0}^{\infty} a_{ij}\cos\lambda_i X \cos\lambda_j Y, \qquad \lambda_i = \pi\left(\tfrac{1}{2} + i\right), \quad i \in \mathbb{Z}. \tag{2.25}$$

which ensures that all boundary conditions are immediately satisfied. To determine the scalar coefficients a_{ij}, we substitute the form of u into (2.24), and use the orthogonality of the cosine function, to determine that

$$a_{ij} = \frac{(-1)^{i+j} 4Mm^2h^2}{(1+m^2)\lambda_i\lambda_j\left(\lambda_i^2+\lambda_j^2\right)}. \tag{2.26}$$

The volume flux Q across the cross-sectional area $A = mh^2$ is found to be $Q = KMh^4$, where K, a scalar constant that only depends on the vertex angle θ, is given by

$$K = \frac{4m^3}{1+m^2}\sum_{i=0}^{\infty}\sum_{j=0}^{\infty}\frac{1}{\lambda_i^2\lambda_j^2\left(\lambda_i^2+\lambda_j^2\right)} \simeq \frac{0.137m^3}{1+m^2}. \tag{2.27a,b}$$

In the non-inclined case $\beta = 0$, we derive

$$2mh\frac{\partial h}{\partial t} - \frac{Kg}{\nu}\frac{\partial}{\partial z}\left(h^4\frac{\partial h}{\partial z}\right) = 0 \tag{2.28}$$

from the local continuity condition (2.7). The global continuity equation (2.11) gives

$$\int_0^{z_N(t)} mh^2\,\mathrm{d}z = V. \tag{2.29}$$

By dimensional analysis of (2.28) and (2.29), or otherwise, we choose a suitable similarity variable

$$\zeta = \left(\frac{4m^5\nu^2}{K^2g^2V^3}\right)^{1/7} zt^{-2/7}. \tag{2.30}$$

Thus, the propagation distance z_N scales like $t^{2/7}$ and is given by

$$z_N = \zeta_N\left(\frac{K^2g^2V^3}{4m^5\nu^2}\right)^{1/7} t^{2/7}, \tag{2.31}$$

where ζ_N is a scalar constant to be determined.

To obtain exact solutions, it is natural to seek a similarity solution h of the form

$$h = \zeta_N^{2/3}\left(\frac{2\nu V^2}{Kmgt}\right)^{1/7}\phi(s), \tag{2.32}$$

where the new independent variable $s = \zeta/\zeta_N$ is a scaled similarity variable which varies between 0 and 1. Substituting (2.32) into (2.28), we obtain

$$\phi(\phi + 2s\phi') + 7(\phi^4\phi')' = 0 \tag{2.33}$$

from the local continuity equation (2.7) with boundary condition $\phi(1) = 0$, and

$$\zeta_N = \left(\int_0^1 \phi^2\,\mathrm{d}s\right)^{-3/7} \tag{2.34}$$

from the global continuity equation (2.11). The solution $\phi = [\frac{3}{14}(1-s^2)]^{1/3}$ is found analytically from which $\zeta_N = (14/3)^{2/7}[B(1/2, 5/3)/2]^{-3/7} \approx 1.768$, where $B(x, y)$ is the beta function. Note that in each of the horizontally spreading cases investigated within a constrained boundary, the structure function of the height h is of the form $(1-s^2)^{1/3}$, for a suitable variable s with $0 < s < 1$ but that the pre-multiplicative factors vary from situation to situation, as do the rates of propagation.

Geometry	Axisymmetric	Two-dimensional		Semi-circular		V-shaped	
Slope	horizontal	horizontal	inclined	horizontal	inclined	horizontal	inclined
δ	1/8	1/5	1/3	1/4	3/7	2/7	1/2
Reference	Ha	Ha	Hb	tp	tp	tp	tp

TABLE 1. Summary of different set-ups of viscous gravity currents and their rate of propagation, where δ denotes the power of time proportional to the propagation distance. References Ha, Hb and tp refer to Huppert (1982*a*), Huppert (1982*b*) and this paper respectively.

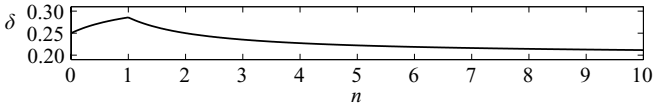

FIGURE 3. Plot of δ against n, where the propagation distance scales as t^{δ} along a horizontal channel with shape $y = a|x/a|^n$.

In the inclined case, the local continuity equation (2.7) becomes

$$m\frac{\partial h}{\partial t} + \frac{2Kg\sin\beta}{\nu}\frac{\partial h}{\partial z}h^2 = 0 \tag{2.35}$$

and the global continuity equation (2.29) remains the same as in the non-inclined case. The same technique is used to find a suitable similarity variable and to derive the solution

$$h = \left(\frac{m\nu}{2Kg\sin\beta}\right)^{1/2} z^{1/2}t^{-1/2}, \quad z_N = \left(\frac{4KgV\sin\beta}{m^2\nu}\right)^{1/2} t^{1/2}. \tag{2.36a, b}$$

A summary of the propagation rates for different set ups is given in table 1. John Lister, on seeing a first draft of this paper, set a question for Part III students in Cambridge that nicely generalizes the results. When a fixed volume is released at the origin at $t = 0$ and spreads along a long straight horizontal channel with the shape $y = a|x/a|^n$, where $n = 1$, 2 and ∞ correspond to V-shaped, semicircular and flat-bottomed set-ups respectively, the propagation distance z_N scales like $t^{(n+1)/(3n+4)}$ for $0 < n \leqslant 1$ and $t^{(n+1)/(5n+2)}$ for $n \geqslant 1$, determined by using (2.7)–(2.11) and scaling arguments. The different expressions arise because the more rapid variation occurs in the fluid width for $0 < n < 1$ and in the fluid depth for $n > 1$. The exponent, as a function of n, has a maximum at $n = 1$ as shown in figure 3.

3. Experimental investigations

To test the theoretical results, we conducted a series of laboratory experiments in which a constant volume of glycerine was released from one closed end of a long container inclined at different angles to the horizontal, with either a semicircular or V-shaped boundary. The volumes of glycerine used were sufficiently large to minimize any effects of surface tension.

In the set-up with semicircular cross-section, a plastic gutter of length 2 m and radius of curvature 5.8 cm was supported on a solid wooden base and braced by aluminium angle bars to prevent it from bending or distorting. For the non-inclined case, thin sheets of cardboard were inserted where necessary underneath the wooden base to obtain an absolutely horizontal channel as indicated by a spirit level. For

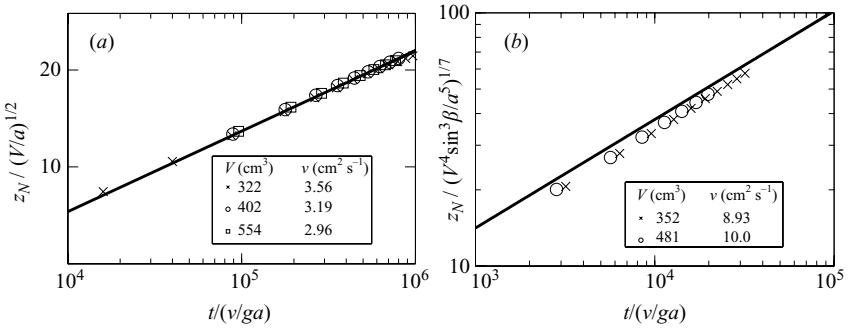

FIGURE 4. Comparison between theory (solid line) and experimental data of non-dimensional distance as a function of non-dimensional time along a semicircular surface that is (*a*) horizontal and (*b*) inclined at an angle of 7°.

FIGURE 5. Photograph from the top of the gravity current propagating 95 cm from right to left along a horizontal semicircular channel, 47 s after 341 cm^3 of glycerine with a viscosity of 3.22 cm^2 s^{-1} was released. The solid white line marks the fluid boundary as predicted by theory.

the inclined case, the wooden base was lifted up at one end and then firmly fixed to obtain an inclination angle of 7°, 15° or 61°.

Before each experimental run, the exact quantity of fluid to be used was implicitly derived by weighing the mass and using the known value of 1.260 g cm^{-3} for the density of glycerine, reasonably independent of its purity. The viscosity of the glycerine was measured accurately to within 1 mm^2 s^{-1} using an U-tube viscometer. This was necessary because of sensitivity to purity and temperature fluctuations between runs.

A lock gate, consisting of a circular disk of radius 5.4 cm with a sponge layer of 1 cm thickness glued onto the rim to fit it inside the gutter, was used to retain the liquid at one closed end of the gutter before it was quickly released. Test runs revealed that initial procedures have litte effect on the resultant flow, as is expected for situations described by similarity solutions, so the liquid was quickly poured into one end without using the lock gate in some experimental runs.

The propagating distance from the closed end of the channel was recorded at regular 5 s intervals after the time of release of the glycerine. The foremost position of the propagating gravity current was directly marked on the channel alongside the current to within 1 mm. Photographs were taken from approximately 50 cm above the propagating current. In figure 4, scaled non-dimensional distance is plotted against non-dimensional time on logarithmic axes and compared with the theoretical curve, for both non-inclined and inclined cases. The data show a very satisfactory collapse and close agreement with the theory, confirming the $t^{1/4}$ (non-inclined) and $t^{3/7}$ (inclined) power-law relationship as well the validity of the pre-multiplicative scaling factors of (2.19*b*) and (2.22). Figure 5 shows a snapshot of the fluid boundary 47 s after release, upon which we have superposed the theoretical curve of width W

$$W(z) = \left[\frac{105\nu R^3}{8gt}(z_N(t)^2 - z^2)\right]^{1/6}, \tag{3.1}$$

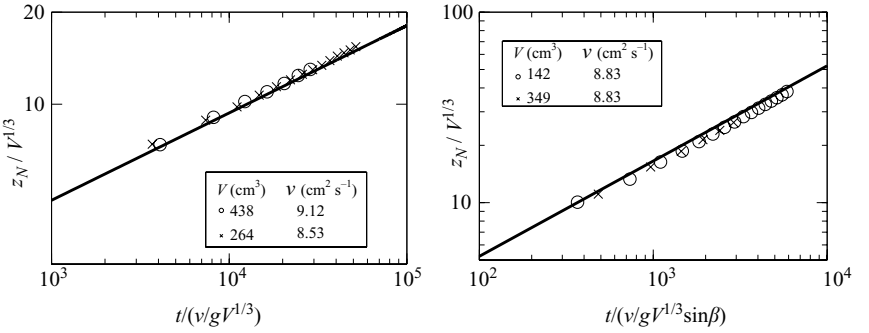

FIGURE 6. Comparison between theory (solid line) and experimental data of non-dimensional distance as a function of non-dimensional time along a V-shaped boundary that is (*a*) horizontal and (*b*) inclined at an angle of 7°.

which is derived from (2.19*a*), where $z_N(t)$ is given by (2.19*b*). Although capillarity effects possibly play a role at the front of the current, where the surface tension influences the thin layer of the slowly propagating nose, as suggested by the discrepancy seen near the front in figure 5, they do not affect our results for the overall shape or the propagation rate, as shown by the very close agreement in figures 4 and 5.

No instability was observed at the front of the current at any time in any of our experiments. Unlike the two-dimensional flows down a slope in which numerous extended regions of fluid developed (Huppert 1982*b*), the fluid did not break up in any of our experimental runs. This may be due to the rapid diminishing of the fluid width W, as given by (3.1), at the front as $z \to z_N$, becoming identically zero at $z = z_N$. Even at large angles of inclination, which might favour an instability, the possible resultant wavelength is greater than the flow width.

In the set-up with a V-shaped boundary, we tested the theoretical model for the special case with vertex angle $\theta = \pi/4$. A rectangular glass container of length 1 m, width 15 cm and height 10 cm was rotated about its long axis by 45° and rested onto heavy metallic V-shaped supports at each end. These supports stood on a wooden base so that the inclination angle could be adjusted. A lock gate was fitted towards one end of the channel using a thin sheet of metal that could slide against the sidewalls into the container. Glycerine was poured into the end from a beaker, which was weighed before and after pouring to record the fluid mass. The lock gate was then quickly lifted to allow the fluid to propagate along the container. The propagation length of the current was again measured at 5 s intervals by marking its foremost position along one sidewall of the container to within 1 mm. In figure 6, non-dimensional distance is plotted against non-dimensional time on logarithmic axes, and compared with the theoretical curve for both non-inclined and inclined results. Propagation as predicted by the theoretical model is clearly in agreement with the experimental results.

4. Conclusion and discussion

We conclude that a variety of different mathematical relationships between propagation distance and time can be obtained by considering different confining boundaries, as summarized in table 1. These results are only valid for the instantaneous release of a fixed volume of viscous fluid. Additional relationships will arise if the

discharge rate is not constant. We are currently investigating both theoretically and experimentally such an extension of our work.

A possible application of our results is to interpret quantitatively lava flows down the flanks of a volcano. As in many real geological situations there are additional effects not considered by the theory. In this case these include: a time-dependent effusion rate; a temperature-dependent viscosity, which increases as the lava flow propagates and cools; non-Newtionian effects; an incline of varying slope; and a growing surface crust as discussed later. Partially because of these additional factors, recourse has often been made to numerical models (Wadge, Young & McKendrick 1994). However, simplified analytical models, as outlined here, act as essential foundations against which the numerical results can be checked and understood.

One of the best observed and documented lava flows is the extrusion from the Lonquimay Volcano, Chile, which erupted almost continuously during 1989 and for a few weeks on either side (Naranjo *et al.* 1992). The authors state that the length of the lava flow down a rough incline ranging in slope from 0.7° to 6.3° decreased exponentially with distance from the vent as a consequence of cooling and the increase of apparent viscosity at the flow front. They determined this apparent viscosity as

$$\mu_a = \rho g h_N^2 \frac{\sin\beta}{3v}, \tag{4.1}$$

which they call the Jeffreys open channel equation, where h_N is the thickness of the flow front which moves with velocity v determined by evaluating the rate of change of the length of the lava as a function of time. By dimensional analysis, (4.1) must be correct; only the premultiplicative constant can depend on the shape of the boundary. Evaluating $h_N \equiv h[z_N(t)]$ from (2.21) and (2.36*a*) and $v = \dot{z}_N(t)$ from (2.22) and (2.36*b*) we find that the constant $1/3 = 0.333$ in (4.1) for open channel flow is replaced by $24/105 = 0.229$ for a circular constraining geometry and $K/m = 0.137m^2/(1+m^2)$ for a V-shaped constrainer. Our numerical alterations to the results of Naranjo *et al.* (1992) make little difference, because the variaton in the determined viscosity with distance was over four orders of magnitude. Nevertheless, our analysis places their results on a firmer footing.

Upon completion of a close-to-final draft of this manuscript Ross Kerr kindly sent us a copy of Kerr & Lyman (2007) which analyses the Lonquimay lava flow based on the concept of a viscous fluid of given width flowing down an incline resisted by the strength of the growing surface crust (rather than by internal viscous effects). Kerr & Lyman state that the results of such a model appear to be in good agreement with the data obtained from the Lonquimay lava flow. We look forward to the application of their concepts to other (less well documented) lava flows, possibly incorporating the inclusion of constraining sidewalls, as examined herein.

We are grateful to Ross Kerr, Steve Sparks and Geoff Wadge for their constructive comments on an earlier draft and to Mark Hallworth for his experimental aid. This research was supported by an EPSRC Summer Bursary for undergraduates in the UK (D.T.) and a Royal Society Wolfson Research Merit Award (H.E.H.).

REFERENCES

Acheson, D. J. 1990 *Elementary Fluid Dynamics.* Oxford University Press.

Acton, J. M., Huppert, H. E. & Worster, M. G. 2001 Two-dimensional viscous gravity currents flowing over a deep porous medium. *J. Fluid Mech.* **440**, 359–380.

Batchelor, G. K. 1967 *An Introduction to Fluid Dynamics.* Cambridge University Press.

HUPPERT, H. E. 1982*a* The propagation of two-dimensional and axisymmetric viscous gravity currents over a rigid horizontal surface. *J. Fluid Mech.* **121**, 43–58.

HUPPERT, H. E. 1982*b* The flow and instability of viscous gravity currents down a slope. *Nature* **300**, 427–429.

HUPPERT, H. E. 2006 Gravity currents : a personal review. *J. Fluid Mech.* **554**, 299–322.

KERR, R. C. & LYMAN, A. W. 2007 The importance of surface crust strength during the flow of the 1988–1990 andesite lava of Lonquimay Volcano, Chile. *J. Geophys. Res.* **112** (in press).

LISTER, J. R. 1992 Viscous flows down an inclined plane from point and line sources. *J. Fluid Mech.* **242**, 631–653.

MEI, C. C. & YUHI, M. 2001 Slow flow of a Bingham fluid in a shallow channel of finite width. *J. Fluid Mech.* **431**, 135–159.

NARANJO, J. A., SPARKS, R. S. J., STASIUK, M. V., MORENO, H. & ABLAY, G. J. 1992 Morphological, structural and textural variations in the 1988–1990 andesite lava of Lonquimay Volcano, Chile. *Geol. Mag.* **129**, 657–678.

SIMPSON, J. E. 1997 *Gravity currents: In the Environment and the Laboratory*. Cambridge University Press.

WADGE, G., YOUNG, P. A. V. & MCKENDRICK, I. K. 1994 Mapping lava flow hazards using computer simulations. *J. Geophys. Res.* **99**, 489–504.